Proceedings of the 11th Polish–Japanese Joint Seminar on Micro and Nano Analysis, Gniew, September 11–14, 2016

Microstructure of Friction Stir Welded Dissimilar Wrought 2017A and Cast AlSi9Mg Aluminum Alloys

M. Kopyściański[a], S. Dymek[a,*], C. Hamilton[b], A. Węglowska[c], A. Pietras[c], M. Szczepanek[a] and M. Wojnarowska[a]

[a]AGH University of Science and Technology, Al. A. Mickiewicza 30, 30-059 Kraków, Poland

[b]Miami University, College of Engineering and Computing, Oxford, Ohio, USA

[c]Instytut Spawalnictwa, Bł. Czesława 16-18, 44-100 Gliwice, Poland

Friction stir welding was applied to join dissimilar aluminum alloys: wrought 2017A and cast AlSi9Mg. The produced weldment was free from cracks and any discontinuities. The weld microstructure was composed of alternating bands of the welded alloys; however, the alloy that was placed on the advancing side (AlSi9Mg) dominated the weld center. The grain size within the particular bands was similar in both alloys. The hardness profile reflected the microstructure formed during welding. The weld microstructure as well as the shape of hardness profile across the weld were justified by numerical simulation of material flow during welding.

DOI: 10.12693/APhysPolA.131.1390

PACS/topics: friction stir welding, aluminum alloys, microstructure

1. Introduction

Friction stir welding (FSW) is already well recognized as a joining technology, however, research and development efforts have been primarily focused on the welding of the same metallic alloys. The investigations of joining dissimilar alloys are much less covered. Only recently, Kumar et al. [1] reviewed and compiled the current state of knowledge regarding this topic. Their work showed that many phenomena occurring during welding of dissimilar alloys call for an explanation and a deeper understanding. The FSW process occurs in solid-state and thus avoids the microstructural and mechanical complications that typically accompany melting and resolidification during fusion welding. The primary difference between the friction stir welding of similar and dissimilar alloys is the discontinuity in physical properties, such as chemical composition, viscosity, thermal conductivity as well as mechanical properties between joining alloys. This promotes an asymmetry in heat generation and material flow during welding across the abutting surfaces [1, 2].

This research was aimed at providing new experimental data to better understand the phenomena that occur during friction stir welding of different aluminum alloys — cast with wrought ones. Additionally, a coupled thermal/flow model was developed to simulate the mechanical mixing of aluminum alloys AlSi9Mg and 2017A that occur during friction stir welding.

2. Material and experimental procedure

Commercial wrought 2017A-T451 and cast AlSi9Mg aluminum alloys with main elements contents given in Table I were friction stir welded at the Welding Institute in Gliwice, Poland. The welds that were subjected to detailed examination were selected after numerous welding experiments with changing welding parameters like welding velocity, rotational speed, vertical force, and the tool shape. All these experiments are described in Refs. [3–5]. The highest weld quality provided the basis for the selection of the appropriate process parameters and type of the tool. Ultimately, the welding was performed with a modified Whorl-type tool made of HS6-5-2 high speed steel with a 24 mm diameter and scrolled shoulder having a 2.5 mm pitch. The pin diameter tapered linearly from 6 mm at the shoulder to 4.5 mm at the tip with an overall height of 5.7 mm. The pin was also threaded with a 3 mm pitch. The tool tilt angle during processing was held constant at 1.5°. The following process parameters were applied: welding velocity — 112 mm/min, rotational speed — 355 rpm and vertical force approximately equal to 32.8 kN. The cast alloy was placed on the advancing side unlike in the works [3–5] where the opposite configuration led to the poor weld quality.

TABLE I

Chemical composition of the alloys 2017A and AlSi9Mg (wt%).

Alloy	Cu	Mg	Mn	Si	Zn	Fe
2017A	4.14	0.72	0.6	0.68	0.18	0.31
AlSi9Mg	0.21	0.31	0.34	0.14	0.14	0.64

The welds were examined using light microscopy with the utilization of polarized light as well as scanning electron microscopy (SEM) with back scattered electrons (imaging and diffraction). Also, a chemical analysis by energy dispersive spectroscopy (EDS) was performed in the SEM. All microstructural examinations were carried out on sections perpendicular to the welding direction on a Zeiss Axio Imager M1m light microscope and on a high resolution FEI Nova NanoSEM scanning electron

*corresponding author; e-mail: gndymek@cyfronet.pl

microscope equipped with a field emission gun and an EDAX system for chemical analysis. The light and scanning electron microstructural studies were supplemented by transmission electron microscopy (TEM). The samples for TEM were excised from both sides of the nugget in the form of 3 mm disks. The disks were thinned on sand papers, dimpled and electropolished in a Struers A8 solution. The observation was carried out on a JEOL 2010 ARP microscope operating at 200 kV. The mechanical examination comprised Vickers hardness as well as tensile testing. The hardness was carried out on the same sections as metallographic examinations. The tests were done on a Wolpert-Wilson Tukon 2500 apparatus. The Vickers results were used for the construction of a hardness profile on a weld cross-section along the line of the mid-thickness plane. The applied load was 1 kg and the distance among testing points was 1.0 mm. The hardness profiles were constructed about one year after welding, i.e. after natural ageing. As was shown in Ref. [6], natural ageing can substantially alter the shape of hardness profiles in age-hardenable aluminum alloys. Tensile tests were performed on three specimens excised from the welded blanks in such a way that the test piece was perpendicular to the weld axis and the weld occupied the central portion of the test piece. The testing was performed on a ZWICK Z250 machine.

In order to comprehensively assess the material flow behavior during the friction stir welding of 2017A and AlSi9Mg alloys, a thermal/flow model was developed with Comsol multi-physics software. The model was based on the simulation presented in Refs. [2, 7].

3. Results and discussion

The microstructure of the produced weld (in macro scale) is presented in Fig. 1.

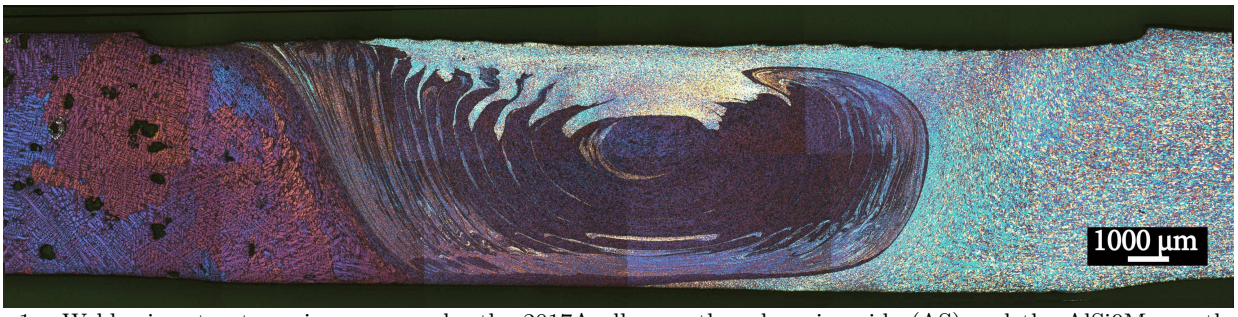

Fig. 1. Weld microstructures in macro scale; the 2017A alloy on the advancing side (AS) and the AlSi9Mg on the retreating side (RS); optical microscope, polarized light.

The left side of Fig. 1 corresponds to the advancing side and shows the microstructure of the as-received cast AlSi9Mg alloy. It is a typical cast microstructure with characteristic large grains filled with Si dendrites. Sporadically large voids, visible as dark stains, are observed. On the other hand, the right side of Fig. 1 corresponds to the retreating side, i.e. the 2017A alloy. The microstructure of this alloy is typical for wrought aluminum alloys subjected to hot working. The grain size in this region is small, about 30 to 40 μm, and recrystallized. The weld microstructure reflects the complexity of the material flow that occurs during the mixing of two different aluminum alloys in solid state. The well-defined volume of mixing (nugget) can be distinguished in the weld region. The distinct boundaries between the stir and thermomechanical zones on the advancing and retreating sides are observed. This is in contrast to welds produced by FSW for the same kind of aluminum alloys where the boundary on the retreating side is rather diffuse — the microstructure of the stir zone continuously changes into the microstructure of the thermomechanical zone [6, 8]. In this regard such a microstructure is very similar to that in the dissimilar FSW joint between 2017A and 7075 aluminum alloys described in Ref. [9] where the same shape of the nugget was observed. The microstructure of the nugget is composed of irregular interleaving bands of the materials being joined revealing their flow pattern around the tool during welding. It was found that the AlSi9Mg alloy, the material from the advancing side, predominantly occupies the central part of the nugget; however, a large portion of the material from the retreating side (2017A alloy) appears in the upper part of the nugget.

Figure 2 presents the banded structure of the nugget on the advancing side observed at higher magnification. The character of these flow patterns resembles the mixing of two dense liquids that do not dissolve in each other. The detailed investigation in SEM provided yet more details regarding the microstructure.

Figure 3 shows the banded structure on an image formed by back scattered electrons. The contrast in such images is sensitive to the mean atomic number of elements occurring in the investigated area (Z-contrast)

Thus, the brighter bands belong to the 2017A alloy since this alloy contains more heavy elements (mainly Cu) and the darker bands to the AlSi9Mg alloy. The white particles represent intermetallic phases that contain Fe, Mn, Cu or a combination of these elements. The grey particles correspond to Si solid solution that was broken down by the tool action during welding. The

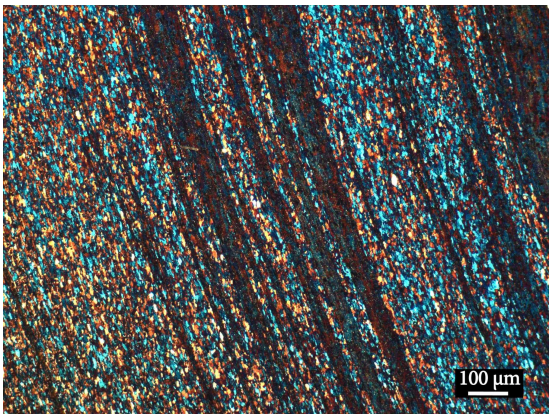

Fig. 2. Banded structure in the stir zone with the large portion of the 2017A alloy occupying advancing side of the nugget; optical microscope, polarized light.

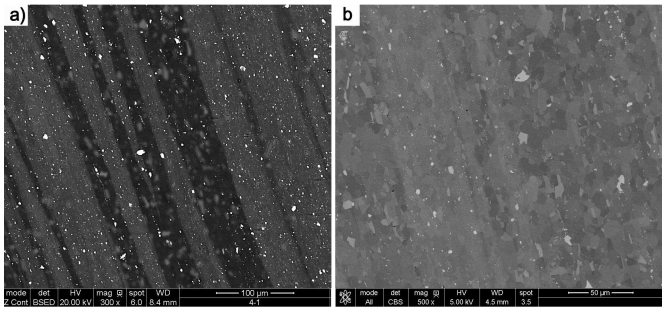

Fig. 3. Microstructure in the stir zone on the advancing side of the nugget; SEM, backscattered electrons: (a) banded structure, Z-contrast, (b) superimposed Z-contrast and orientation contrast.

image in Fig. 3b shows also an orientation contrast produced by backscattered electrons. It is shown that the grain size in both alloys constituting the nugget is similar.

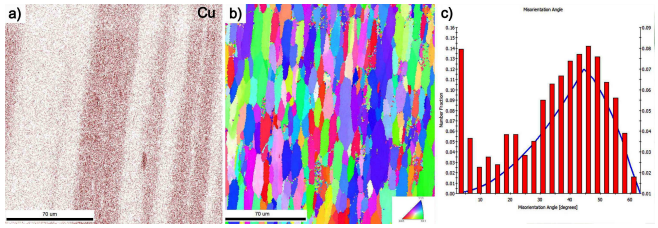

Fig. 4. EDS map and EBSD analysis of the nugget area on the retreating side: (a) orientation image, (b) Cu map, (c) misorientation angle distribution with the Mackenzie plot.

The SEM imaging is confirmed by EDS mapping (Fig. 4a) showing that the different amount of Cu in the investigated alloys produces different contrast. The orientation map constructed by electron back scattered diffraction (EBSD) is presented in Fig. 4b and the histogram of grain boundary misorientation angles together with the Mackenzie plot — in Fig. 4c. As shown in Fig. 4b, the bands exhibit similar grain sizes and shapes. The grains in this region (the nugget on the advancing side) are elongated in the direction of the material flow during mixing. This shape may suggest that the material is textured and not fully recrystallized. However, the distribution of the misorientation angles between grains shows that the majority of grain boundaries exhibit a high angle character (20−60°). This distribution corresponds more or less to the Mackenzie plot [10].

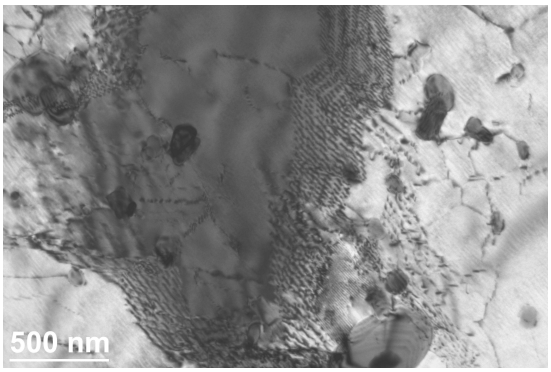

Fig. 5. Dislocation arrangements in the weld nugget.

Since the Mackenzie plot represents the distribution of misorientation angles for a randomly textured cubic polycrystal, it suggests that despite heavy deformation in the stir zone and dynamic recovery and recrystallization occurring in this region due to high temperature the crystallographic texture is very weak. As such, and taking into account that quite a lot of boundaries exhibit a low angle character, the elongated shape of grains on the orientation image may result from clustering of subgrains with similar orientation. However, the misorientation between these subgrains is likely smaller than 2°. Otherwise, it should have been detected on the EBSD pattern. Indeed, the TEM studies show that a large number of dislocations is present in the microstructure and some of the dislocations are arranged in sub-boundary configurations with very small misorientation (Fig. 5). The TEM images also revealed a substantial number of particles that was present within the nugget region. It was characteristic that particles found inside the cast alloy bands exhibited irregular shapes that resulted from the fracturing of large Si and intermetallic particles.

The mechanism of breaking large intermetallic particles is shown in Fig. 6. The image of the microstructure presented in Fig. 6 was produced by backscattered electrons with utilization of both composition and orientation contrast. Thus white particles correspond to an intermetallic phase containing heavy elements and irregular grey particles correspond to an Si phase. The general conclusion from the TEM study is that the microstructure in the nugget is highly recovered but it is not fully recrystallized.

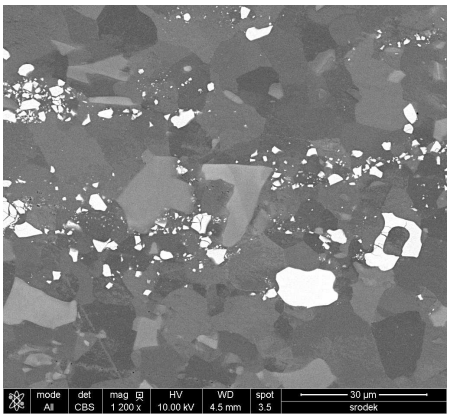

Fig. 6. Refinement of hard particles in the cast AlSi9Mg alloy.

The hardness profile of the weld is shown in Fig. 7. The hardness of the base materials was 80 HV1 and 136 HV1 for the AlSi9Mg and 2017A alloys respectively. The profile reflects the microstructure of the weld shown in Fig. 1. The local maximum on the advancing side corresponds to the left side of nugget where a high density of the bands of the 2017A alloy occur. The tensile strength was 132 MPa. All samples broke within the cast alloy outside the weldment. The elongation was below 1%.

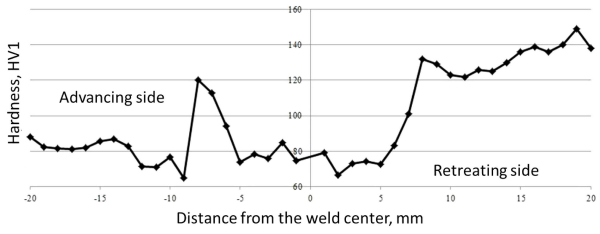

Fig. 7. Hardness profile across the nugget in the mid-thickness plane.

Within the numerical simulation, material tracers are released from a position ahead of the tool on either side of the weld centerline at several time intervals. Surface material tracers ($z = 1$ mm) from the advancing and retreating sides of the weld are initially swept toward the retreating side with the scroll of the tool shoulder directing their flow toward the tool center. Under the influence of the tool pin, the surface tracers flow down into the material thickness adjacent to the pin. The majority of surface material that is introduced into the workpiece rotates around the pin and remains within a zone that extends to ≈ 5 mm on either side of the weld centerline. Tracers initially located at the mid-plane thickness ($z = 3$ mm) follow the tool rotation, but flow up toward the workpiece surface as they rotate. This flow region begins at approximately 7 mm from the centerline and extends out to 9 mm, essentially surrounding the surface material zone described above. Given the downward flow of surface material into the workpiece thickness, a complementary upward flow of material surrounding is not surprising. Such flow behavior gives rise to the alternating layers of AlSi9Mg and 2017A within the process zone as seen in the micrograph of Fig. 1. Materials tracers initially located at the bottom plane of the workpiece thickness ($z = 5$ mm) also reveal a strong upward flow to the workpiece surface where material is "recaptured" by the tool shoulder and then pulled back into the workpiece thickness by the pin. The material flow significantly affects the final microstructure of the weld nugget and, therefore, its hardness profile. The nugget is ultimately composed of regions of AlSi9Mg and 2017A with unique temperature histories depending on the material's initial location within the joint cross-section.

4. Summary

The friction stir welding of dissimilar aluminum alloys carried out at carefully selected welding conditions produces sound welds without any welding discontinuities. The weld microstructure is composed of alternating bands of the welded alloys. However, the AlSi9Mg alloy that was located on the advancing side dominates in the weld center. The hardness profile across the weld correlates strictly with the microstructure. The weld microstructure as well as the hardness profile across the weld are justified by numerical simulation of material flow during welding.

Acknowledgments

This work was support by the Polish National Science Center, grant No. 2013/11/B/ST8/04409.

References

[1] N. Kumar, R.S. Mishra, W. Yuan, *Friction Stir Welding of Dissimilar Alloys and Materials*, Butterworth-Heinemann (Elsevier), Oxford 2015.

[2] C. Hamilton, M. Kopyściański, O. Senkov, S. Dymek, *Metall. Mater. Trans. A* **44**, 1730 (2013).

[3] K. Mroczka, A. Pietras, in: *9th Int. Symp. on Friction Stir Welding, Huntsville (USA)*, 2012, TWI Ltd., Cambridge (UK) 2012, p. 876.

[4] K. Mroczka, A. Pietras, in: *Proc. Mater. Sci. Technol. Conf. Exhibition 2012, Pittsburgh*, Association for Iron & Steel Technology, Warrendale 2012, p. 308.

[5] K. Mroczka, *Arch. Metall. Mater.* **57**, 1293 (2014).

[6] I. Kalemba, C. Hamilton, S. Dymek, *Mater. Des.* **60**, 295 (2014).

[7] C. Hamilton, M. Kopyściański, A. Węglowska, S. Dymek, A. Pietras, *Metall. Mater. Trans. A* **47**, 4519 (2016).

[8] I. Kalemba, S. Dymek, C. Hamilton, M. Blicharski, *Mater. Sci. Technol.* **27**, 903 (2011).

[9] M. Kopyściański, A. Węglowska, A. Pietras, C. Hamilton, S. Dymek, *Key Eng. Mater.* **682**, 31 (2016).

[10] J.K. MacKenzie, *Biometrika* **45**, 229 (1958).